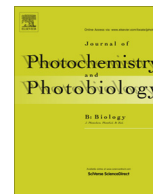




Contents lists available at ScienceDirect

Journal of Photochemistry and Photobiology B: Biology

journal homepage: www.elsevier.com/locate/jphotobiol

Bioimaging, antibacterial and antifungal properties of imidazole-pyridine fluorophores: Synthesis, characterization and solvatochromism

N. Nagarajan^a, G. Vanitha^a, D. Arul Ananth^b, A. Rameshkumar^b, T. Sivasudha^b, R. Renganathan^{a,*}^a School of Chemistry, Bharathidasan University, Tiruchirappalli 620024, Tamil Nadu, India^b Department of Environmental Biotechnology, Bharathidasan University, Tiruchirappalli 620024, Tamil Nadu, India

ARTICLE INFO

Article history:

Received 28 May 2013

Received in revised form 21 August 2013

Accepted 26 August 2013

Available online 5 September 2013

Keywords:

Imidazole

Pyridine

Solvatochromism

Bioimaging

Antibacterial

ABSTRACT

A series of imidazole derivatives connected with pyridine moiety through phenyl groups were synthesized by using Suzuki coupling followed by multicomponent cyclization reaction. Results obtained from spectroscopic (¹H NMR, ¹³C NMR, Mass) and single crystal X-ray diffraction analysis of synthesized compound was in very good agreement with its chemical structure. UV–Vis and fluorescence studies in various solvents with different polarity demonstrated that these compounds were sensitive to the polarity of the microenvironment. In addition, multi linear regression analysis based on Kamlet–Taft and Catalán new four parameter solvent scale results in solvatochromism and was mainly influenced by solvent polarisability and dipolarity of the environment. The electrochemical stability of the compounds was also studied by cyclic voltammetry. An excellent fluorescent nature with high quantum efficiency of the compounds was successfully utilized to probe the bacteria by using fluorescence microscopy. In addition, the antibacterial and antifungal activity of these compounds were also studied *in vitro* by the disk diffusion assay against one Gram-positive, three Gram-negative bacteria and *Candida albicans*. MPBI showed relatively good inhibitory action against Gram-negative bacteria and TPBI against Gram-positive bacteria and 3PBI against *C. albicans*.

© 2013 Elsevier B.V. All rights reserved.

1. Introduction

The heterocyclic compounds constitute an important group in modern organic chemistry, not only because of their abundance, but also primarily because of their chemical, biological and optoelectronics significance. Imidazole is an important family of heterocyclic compounds with a broad interest owing to their bioactive properties. Indisputably, imidazole derivatives showed a broad range of bioactivities (for example: antiinflammatory, anticancer, appetite stimulant activity, antitumor and antifungal, etc.) [1,2]. Consequently, numerous efforts in the recent decades have been focused on the preparation of those privileged scaffolds. Moreover, imidazoles are key systems in nature (for example, histidine, and vitamin B12, and as a component in DNA base-pair structure, biotin, etc.) [3]. Other important applications in recent year include dye sensitized solar cells (DSSCs) [4,5], nonlinear optics (NLO) [6–9], organic light emitting diodes (OLED) [10–13]. Interestingly, substituted imidazole derivatives showed excellent fluorescent behavior that has been successfully utilized to sense the ions by using simple, cost effective fluorescent sensor

applications [14–18]. Indeed, outstanding solvatochromic behavior of the imidazole derivatives have also been explored which could be very useful in sensing the change of microenvironment in biology [19,20]. Therefore, fluorophore with microenvironment sensitivity as well as excellent emissive nature with a predictable photophysical property in relation to their structure is highly desirable for biochemical applications. Apart from this, the steadily increasing bacterial resistance to existing drugs is a serious problem in antibacterial therapy and necessitates continuing research into new classes of antibacterial [21,22]. In view of this, the work presents synthesis of various mono and bis-imidazole derivatives conjugated with another heterocyclic moiety namely pyridine. Further, synthesized compounds were characterized using NMR, mass and single crystal X-ray diffraction (one of the compound, TPBI) techniques. It is also a fundamental academic interest to study the optical and electrochemical properties of the compounds, thus the absorption and emission behavior of the compounds were analyzed in different solvents with varying polarity. The solvatochromic behavior was correlated with Lippert–Metaga, Kamlet–Taft and Catalán's new four parameter solvent scales. The fluorescence nature of the compounds was successfully utilized to probe the bacteria by using fluorescence microscopic techniques. Further,

* Corresponding author. Tel.: +91 431 2407053; fax: +91 431 2407045.

E-mail address: rengas@gmail.com (R. Renganathan).

the antibacterial and antifungal activities of the compounds were also explored.

2. Experimental section

2.1. Reagents and instruments

All the chemicals were commercially available and they were used without further purification. ^1H NMR and ^{13}C NMR were recorded on a Bruker Avance 400 (400 MHz) NMR spectrometer. Dimethylsulfoxide (DMSO- d_6) and CDCl_3 were used as solvent and tetramethylsilane (TMS) as internal standard. Mass spectra were obtained on a FDMS, VG Instruments ZAB-2 mass spectrometer. X-ray crystallographic diffraction data were collected on a Bruker SMART APEX-II CCD diffractometer at room temperature using graphite-monochromated Mo $K\alpha$ radiation ($\lambda = 0.71073 \text{ \AA}$). Integration and cell refinement were carried out using Bruker SAINT. The structures were solved by direct methods (SHELXS 86/SHELXS 97) and refined by full-matrix least squares on F^2 using SHELXL 97. All non-hydrogen atoms were refined anisotropically. MERCURY was used for all graphical representation of the results. UV–Vis spectra were recorded at room temperature in quartz cuvettes using JASCO V360 spectrophotometer for chloroform (CHCl_3), ethylacetate (EtOAc), tetrahydrofuran (THF), dichloromethane (DCM), ethanol (EtOH), methanol (MeOH), acetonitrile (MeCN), N,N-dimethylformamide (DMF) and dimethyl sulfoxide (DMSO) solutions. Fluorescence spectra were obtained from PerkinElmer LS55 spectrofluorometer in the above mentioned solvents. Solvents of the highest available quality (Spectroscopic or HPLC grade) were used. Emission spectra were recorded by exciting the samples at their absorption maximum unless otherwise mentioned. All the experiments were performed at room temperature at a concentration of 10^{-5} M. Quantum yield of the dyes were calculated by following standard procedure and using 9, 10-diphenylanthracene ($\Phi_f = 0.95$ in ethanol) as Ref. [23] by using the following equation:

$$\Phi_f = \Phi_R \frac{I_S \times OD_R \times n_S^2}{I_R \times OD_S \times n_R^2} \quad (1)$$

where Φ_R is the fluorescence quantum yield of reference, I_S and I_R are the area of the sample and reference under the emission spectrum, OD_R and OD_S are the optical density at the excitation wavelength of the reference and sample, n_S and n_R are refractive index of solvent of sample and reference. In all measurements, the optical density of solutions does not exceed 0.1. The electrochemical properties were investigated by cyclic voltammetry (CV) in DMF by using 0.1 M tetrabutylammonium hexafluorophosphate (TBAPF_6) as supporting electrolyte. The experiments were performed at room temperature (1 mM concentration) with a three-electrode cell consisting of a platinum wire as an auxiliary electrode, a saturated Ag/Ag^+ reference electrode and a platinum working electrode.

The multiple linear regression approach of Kamlet–Taft [24,25] and Catalán [26,27] new generalized solvent polarity scale (four parameter) has been used to correlate UV–Vis absorption and emission energies with an index of the solvent dipolarity/polarizability which is a measure of the solvent's ability to stabilize a charge or dipole through nonspecific dielectric interactions (π^* or SP/SdP), and indices of the solvent's hydrogen-bond donor strength (α or SA) and hydrogen-bond acceptor strength (β or SB) according to the following equations:

$$y_{A,F} = y_0 + a_{\pi^*} \times \pi^* + b_{\alpha} \times \alpha + c_{\beta} \times \beta \quad (\text{Kamlet–Taft equation}) \quad (2)$$

$$y_{A,F} = y_0 + a_{SA} \times SA + b_{SB} \times SB + c_{SP} \times SP + d_{SdP} \times SdP \quad (\text{Catalan equation}) \quad (3)$$

where $y_{A,F}$ denotes a solvent-dependent physicochemical property of absorbance and fluorescence in a given solvent and y_0 the statistical quantity corresponding to the value of the property in the gas phase. SP (solvent polarisability), SdP (solvent dipolarity), SA and SB represent independent solvent parameters accounting for various types of solute–solvent interactions. a_{SA} , b_{SB} , c_{SP} and d_{SdP} are adjustable coefficients that reflect the sensitivity of physical property y in a given solvent to the various solvent parameters.

2.2. Synthesis

2.2.1. General procedure for the synthesis of 4,4'-pyridine-2,6-diyl dibenzaldehyde (3) and 4,4'-pyridine-3,5-diyl dibenzaldehyde (4)

The corresponding dibromopyridine (1 or 2) (1 g, 4.2 mmol) were treated with 4-formylphenylboronic acid (1.33 g, 8.86 mmol), $\text{Pd}[\text{PPh}_3]_4$ (0.487 g, 0.42 mmol), K_2CO_3 (3.4 g, 25.2 mmol) in 5:1 mixture of THF and water and stirred at 70°C under nitrogen atmosphere for 12 h and TLC was used to check the completion of the reaction. The product was extracted with DCM, dried over Na_2SO_4 and the compound was purified by column chromatography (silica gel 60–120 mesh, hexane/EtOAc) (9:1 v/v) as a eluent to afford the desired compound 3 or 4 [28].

2.2.2. 4,4'-Pyridine-2,6-diyl dibenzaldehyde (3)

Yield: 66%, ^1H NMR (400 MHz, CDCl_3): δ_{H} 7.83–7.85 (d, 2H), 7.91–7.95 (t, 1H), 8.02–8.04 (d, 4H), 8.31–8.33 (d, 4H), 10.11 (s, 2H); ^{13}C NMR (400 MHz, CDCl_3): δ_{C} 120.33, 127.54, 130.16, 136.62, 138.05, 144.54, 155.62, 191.95.

2.2.3. 4,4'-Pyridine-3,5-diyl dibenzaldehyde (4)

Yield: 69%, ^1H NMR (400 MHz, CDCl_3): δ_{H} 7.82 (d, 2H, 7.6 Hz), 7.90 (t, 1H, 8 Hz), 8.01 (d, 4H, 8.4 Hz), 8.31 (d, 4H, 8 Hz), 10.09 (s, 2H); ^{13}C NMR (400 MHz, CDCl_3): δ_{C} 120.44, 127.65, 130.27, 136.27, 136.71, 138.16, 144.65, 155.74, 192.06.

2.2.4. General procedure for the synthesis of bis-[4-(4,5-diphenyl-1H imidazol-2-yl)-phenyl]-pyridines (2PBI and 3PBI)

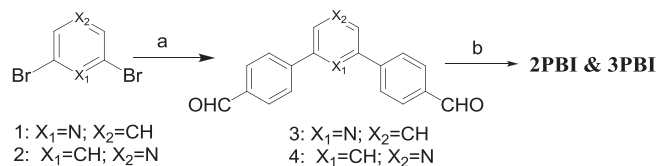
A mixture of $\text{NH}_4 \text{OAc}$ (1.07 g, 13.9 mmol), benzil (0.73 g, 3.48 mmol), and 3 or 4 (0.5 g, 1.74 mmol) in AcOH (6 ml) were refluxed for 4 h. The mixture was poured into cooled water and filtered, washed with water, dried in vacuo and the compound was purified by column chromatography (silica gel 60–120 mesh, hexane/EtOAc) (4:1 v/v) as a eluent to afford the target compound 2PBI and 3PBI as a colorless solid.

2.2.5. 2,6-Bis-[4-(4,5-diphenyl-1H imidazol-2-yl)-phenyl]-pyridine (2PBI)

Yield: 60%, mp: $227\text{--}230^\circ\text{C}$, ^1H NMR (400 MHz, DMSO- d_6): δ_{H} 7.32 (d, 4H, 7.2 Hz), 7.38 (m, 8H), 7.56 (d, 8H, 7.2 Hz), 8.02 (s, 3H), 8.27 (d, 4H, 8.4 Hz), 8.37 (d, 4H, 8.8 Hz), 13.01 (s, 2H); ^{13}C NMR (400 MHz, DMSO- d_6): δ_{C} 118.98, 125.17, 125.51, 126.98, 127.21, 127.79, 128.23, 128.41, 128.64, 130.84, 138.19, 138.32, 145.08, 155.18, 171.96; MS (HRMS) m/z: calculated 667.2736, found 668.2812 (MH^+).

2.2.6. 3,5-Bis-[4-(4,5-diphenyl-1H imidazol-2-yl)-phenyl]-pyridine (3PBI)

Yield: 60%, mp: 215°C , ^1H NMR (400 MHz, DMSO- d_6): δ_{H} 7.35 (broad, 12H), 7.55 (d, 8H, 7.6 Hz), 8.03 (d, 4H, 8.4 Hz), 8.25 (d, 4H, 8.4 Hz), 8.49 (m, 1H), 8.98 (s, 2H), 12.80 (s, 2H); ^{13}C NMR (400 MHz, DMSO- d_6): δ_{C} 119.48, 125.67, 126.01, 127.48, 127.71, 128.29, 128.73, 128.91, 129.14, 131.34, 138.69, 138.82, 145.58, 155.68, MS (HRMS) m/z: calculated 667.2736, found 668.2810 (MH^+).



Scheme 1. Reagents and conditions: (a) Suzuki coupling: 4-formylphenylboronic acid, K_2CO_3 , $Pd[PPh_3]_4$, THF, H_2O , $70^\circ C$, 12 h; (b) benzil, NH_4OAc , AcOH, reflux, 4 h;

2.2.7. General procedure for the synthesis of 4-(6-Bromo-pyridin-2-yl)-benzaldehyde (7)

4-Formylphenylboronic acid (0.7 g, 4.64 mmol) was treated with **1** (1 g, 4.2 mmol) in THF:water (5:1) solvents mixture, $Pd[PPh_3]_4$ (0.24 g, 0.21 mmol), K_2CO_3 (1.72 g, 12.6 mmol) and stirred at $70^\circ C$ for 12 h. The completion of the reaction was monitored by TLC. The mixture is extracted with DCM and dried over Na_2SO_4 . The compound was purified by column chromatography (silica gel 60–120 mesh, hexane/EtOAc) (4:1 v/v) as an eluent to afford the compound **7** as a solid [29].

2.2.8. 4-(6-Bromo-pyridin-2-yl)-benzaldehyde (7)

Yield: 72%, 1H NMR (400 MHz, $CDCl_3$): δ_H 7.701–7.721 (d, 2H), 7.762–7.782 (d, 2H), 7.957–7.990 (m, 1H), 8.038–8.048 (t, 1H), 8.683–8.773 (q, 1H), 10.06 (s, 1H); ^{13}C NMR (400 MHz, $CDCl_3$): δ_C 121.10, 127.85, 128.01, 130.35, 130.51, 136.21, 136.22, 136.88, 137.08, 142.05, 146.42, 150.45, 191.49.

2.2.9. General procedure for the synthesis of 4-[6-(4-tert-Butyl-phenyl)-pyridin-2-yl]-benzaldehyde (8) and 4-[6-(4-Methoxy-phenyl)-pyridin-2-yl]-benzaldehyde (9)

Compound **7** (0.5 g, 1.92 mmol) was reacted through Suzuki coupling with 4-tert-butylphenylboronic acid (0.34 g, 1.92 mmol) or 4-methoxyphenylboronic acid (0.29 g, 1.92 mmol) as mentioned

above. The mixture was extracted with DCM and dried over Na_2SO_4 . The compound was purified by column chromatography (silica gel 60–120 mesh, hexane/EtOAc) (9:1 v/v) as an eluent to afford the compound **8** and **9** as a solid.

2.2.10. 4-[6-(4-tert-Butyl-phenyl)-pyridin-2-yl]-benzaldehyde (8)

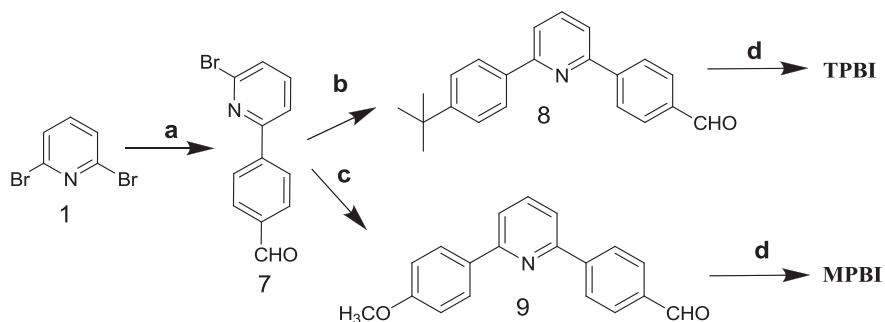
Yield: 78%, 1H NMR (400 MHz, $CDCl_3$): δ_H 1.56 (s, 9H), 6.97 (s, 2H), 7.24 (d, 2H, 7.6 Hz), 7.76 (d, 1H, 8 Hz), 7.86 (t, 1H, 8 Hz), 7.95 (d, 2H, 8 Hz), 8.22 (d, 2H, 8 Hz), 10.07 (s, 1H); ^{13}C NMR (400 MHz, $CDCl_3$): δ_C 20.36, 21.12, 118.93, 124.28, 127.64, 128.50, 130.09, 135.76, 136.35, 137.06, 137.66, 137.72, 145.15, 155.57, 160.23, 192.08. MS (HRMS) m/z: calculated 315.1623, found 316.1656 (MH) $^+$.

2.2.11. 4-[6-(4-Methoxy-phenyl)-pyridin-2-yl]-benzaldehyde (9)

Yield: 81%, 1H NMR (400 MHz, $CDCl_3$): δ_H 3.87 (s, 3H), 7.01–7.03 (d, 2H), 7.67–7.68 (d, 2H), 7.76–7.81 (m, 1H), 7.97–7.99 (d, 2H), 8.09–8.11 (d, 2H), 8.28–8.30 (d, 2H), 10.07 (s, 1H); ^{13}C NMR (400 MHz, $CDCl_3$): δ_C 29.71, 55.39, 114.17, 114.83, 116.05, 1118.59, 118.91, 127.49, 128.02, 128.29, 130.11, 131.74, 1136.40, 137.62, 145.20, 155.08, 156.91, 160.75, 192.06. MS (HRMS) m/z: calculated 289.1103, found 290.1134 (MH) $^+$.

2.2.12. General procedure for the synthesis of 2-(4-tert-Butyl-biphenyl)-6-[4-(4,5-diphenyl-1H-imidazol-2-yl)-phenyl]-pyridine (TPBI) and 2-[4-(4,5-Diphenyl-1H-imidazol-2-yl)-phenyl]-6-(4-methoxy-biphenyl-4-yl)-pyridine (MPBI)

A mixture of NH_4OAc (0.97 g, 12.6 mmol), benzil (0.4 g, 1.9 mmol), and **8** or **9** (0.5 g, 1.73 mmol) in AcOH (6 ml) was heated at $120^\circ C$ for 4 h. The mixture was poured into cooled water and filtered, washed with water, dried in vacuo and the compound was purified by column chromatography (silica gel 60–120 mesh,



Scheme 2. Reagents and conditions: (a) Suzuki coupling: 4-formylphenylboronic acid, K_2CO_3 , $Pd[PPh_3]_4$, THF, H_2O , $70^\circ C$, 12 h; (b) Suzuki coupling: 4-tert-Butylphenylboronic acid; (c) 4-methoxyphenylboronic acid; (d) benzil, NH_4OH , AcOH, reflux, 4 h;

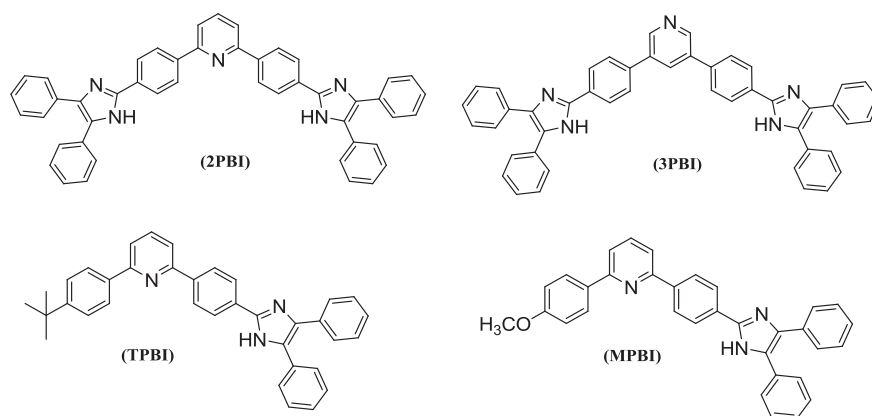


Fig. 1. Structures of the synthesized fluorophores.

hexane/EtOAc) (4:1 v/v) as an eluent to afford the target compound TPBI & MPBI as a colorless solid.

2.2.13. 2-(4-*tert*-Butyl-biphenyl)-6-[4-(4,5-diphenyl-1H-imidazol-2-yl)-phenyl]-pyridine (TPBI)

Yield: 53%, mp: 247 °C, ^1H NMR (400 MHz, DMSO- d_6): δ_{H} 1.323 (s, 9H), 7.37 (t, 1H, 7.2 Hz), 7.31 (t, 2H, 7.2 Hz), 7.37 (t, 1H, 7.2 Hz), 7.45 (t, 2H, 7.2 Hz), 7.53 (d, 4H, 8.4 Hz), 7.59 (d, 2H, 7.6 Hz), 7.86 (d, 1H, 7.6 Hz), 7.91–7.98 (m, 2H), 8.12 (m, 2H, 8.4 Hz), 8.26 (d, 2H, 8.4 Hz), 8.33 (d, 2H, 8.6 Hz), 12.834 (s, 1H); ^{13}C NMR (400 MHz, DMSO- d_6): δ_{C} 31.01, 34.36, 118.51, 118.68, 125.16, 125.46, 125.52, 126.42, 126.54, 126.86, 127.10, 127.81, 128.16, 128.48, 128.63, 128.85, 130.85, 131.02, 135.11, 136.02, 137.45, 138.16, 138.23, 1145.11, 151.70, 155.01, 155.81; MS (HRMS) m/z : calculated 505.6514, found 506.2579 (MH) $^+$.

2.2.14. 2-[4-(4,5-Diphenyl-1H-imidazol-2-yl)-phenyl]-6-(4'-methoxybiphenyl-4-yl)-pyridine (MPBI)

Yield: 58%, mp: 250 °C, ^1H NMR (400 MHz, DMSO- d_6): δ_{H} 3.88 (s, 3H), 7.33 (d, 2H, 6.8 Hz), 7.35 (m, 6H), 7.49 (m, 2H), 7.70 (m, 4H), 7.80 (t, 1H, 8 Hz), 8.04 (d, 2H, 8.8 Hz), 8.10 (d, 2H, 9.2 Hz), 8.13 (d, 2H, 7.2 Hz); ^{13}C NMR (400 MHz, DMSO- d_6): δ_{C} 60.45, 119.39, 123.29, 123.35, 130.73, 131.82, 132.12, 132.37, 133.08, 133.27, 133.44, 133.75, 133.90, 136.08, 136.28, 136.42, 140.38, 142.71, 143.38, 143.56, 150.40, 160.17, 160.76, 165.50; MS (HRMS) m/z : calculated 479.5711, found 480.2060 (MH) $^+$.

2.3. Antimicrobial and fluorescence microscopic studies

2.3.1. Test organisms

Escherichia coli (MTCC 2939), *Pseudomonas aeruginosa* (MTCC 1934), *Rhodococcus rhodochrous* (MTCC 265), *Aeromonas hydrophila* (MTCC 1739), *Candida albicans* (MTCC 227) were obtained from Microbial Type Culture Collection (MTCC), Institute of Microbial Technology (IMTECH), Chandigarh.

2.3.2. Disc diffusion method

The antimicrobial activity of the newly synthesized compounds 3PBI, TPBI and MPBI were investigated through disc diffusion method [30]. An *in vitro* antimicrobial activity was scrutinized against five pathogenic organisms. The actively growing culture suspension was adjusted with peptone water so as to obtain a turbidity that could be visually comparable with 0.5 MacFarland standard which has been prepared by adding 0.5 ml of 0.048 barium chloride with 99.5 ml of 0.36 N sulfuric acid. The turbidity is approximately equal to $1-2 \times 10^8$ CFU/ml. The test compound was dissolved in dimethyl sulfoxide. Freshly prepared mueller hinton agar (MHA) plate was swabbed with microorganisms. Sterile discs (6 mm) were placed over surface of the agar plates followed by the addition of 30 μl (1 mM concentration) of synthesized compounds (3PBI, TPBI and MPBI). The plates were incubated at 37 °C for 12 h and the zone of inhibition measured after the incubation. Experiments were triplicates and standard deviation was calculated. For fluorescence microscopic study, *E. coli* culture was

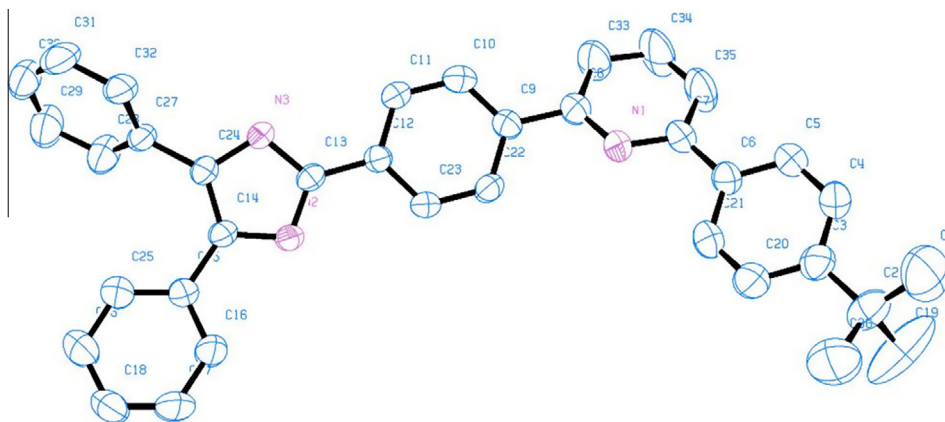


Fig. 2. Crystal structure of TPBI with a thermal ellipsoid plot (50% probability).

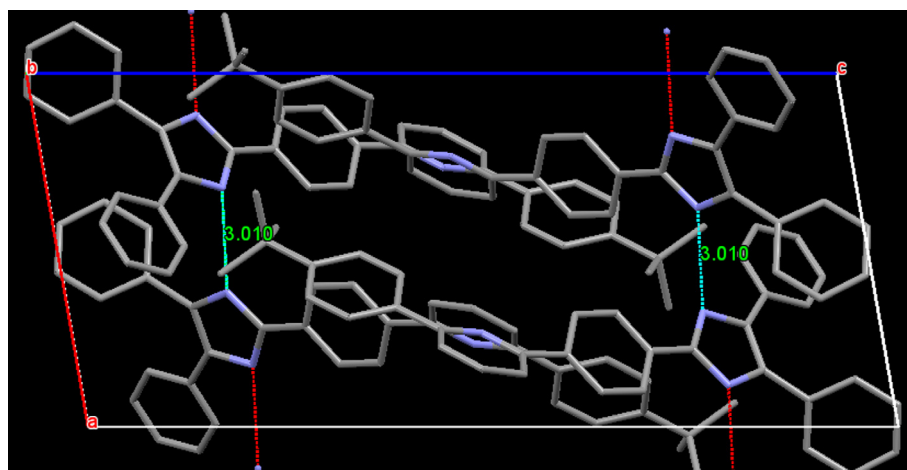


Fig. 3. Crystal packing view along *b* axis.

Table 1
Crystal data and structure refinement for TPBI.

Empirical formula	C ₃₆ H ₃₁ N ₃
Formula weight	505.65
Temperature	296(2) K
Wavelength	0.71073 Å
Crystal system, space group	Triclinic, P-1
Unit cell dimensions	$a = 9.6699(11)$ Å $\alpha = 89.956(6)$ deg. $b = 13.300(2)$ Å $\beta = 80.094(6)$ deg. $c = 21.829(4)$ Å $\gamma = 89.990(5)$ deg.
Volume	$2765.5(7)$ Å ³
Z, Calculated density	4, 1.213 g cm ⁻³
Absorption coefficient	0.071 mm ⁻¹
F(000)	1070
Crystal size	0.40 × 0.30 × 0.25 mm
Theta range for data collection	0.95–28.21 deg.
Limiting indices	$-7 < h < 12$, $-16 < k < 17$, $-28 < l < 28$
Reflections collected/unique	18,584/12,816 [$R(\text{int}) = 0.0492$]
Completeness to theta = 28.21	94.2%
Max. and min. transmission	0.9824 and 0.9721
Refinement method	Full-matrix least-squares on F^2
Data/restraints/parameters	12,816/0/709
Goodness-of-fit on F^2	0.948
Final R indices [$I > 2\sigma(I)$]	$R1 = 0.0841$, $wR2 = 0.2035$
R indices (all data)	$R1 = 0.2038$, $wR2 = 0.2879$

incubated with the compound MPBI (1:1 v/v) for 5 h at 37 °C and washed with phosphate buffered saline (PBS – pH 7.4), three times to remove any unbound fluorophores. Individual aliquots of 30 µl were withdrawn and placed over microscopic slides and observed under a microscope after air drying. The images were acquired under fluorescent (Hund Wetzlak) microscopes. The control for anti-bacterial and antifungal activity were Erythromycin (15 mcg/disc) and Itraconazole (10 mcg/disc) respectively.

3. Results and discussion

3.1. General synthesis

The synthetic procedures of the compounds 2PBI, 3PBI, TPBI and MPBI are shown in Schemes 1 and 2. The structures of the new fluorophore are illustrated in Fig. 1. The first step of the synthesis was Suzuki coupling of corresponding dibromopyridine with 4-formylphenyl boronic acid followed [28] by coupling of methoxy and tertiary butyl phenyl boronic acid [29] (for MPBI and TPBI). Finally condensation of benzil with aldehyde in presence of ammonium acetate and acetic acid results in corresponding target compounds [31,32]. The structures of all the synthesized compounds were characterized by NMR, Mass, and also compound TPBI was confirmed by single crystal X-ray diffraction techniques.

3.2. Crystal structure

The molecular structure of TPBI was determined by single crystal X-ray crystallography. Fig. 2 shows the ORTEP drawing of TPBI. The compound was crystallized in a triclinic crystal system in the P-1 space group. The torsion angle between the imidazole ring and C4-phenyl ring (59.2°) suggests that the phenyl ring is more twisted. Contrastingly, the observed less torsion angle values of phenyl ring attached at C5 (2.2°) & C2 (2.58°) position of imidazole ring suggests that the molecular frame work of the phenyl groups are in plane which would facilitate to maintain the π -conjugation. Similarly, the torsion angle of phenyl group attached with pyridine group is 33.4° & 25.5° also confirms that the conjugation maintain throughout the entire moiety. Moderate intermolecular hydrogen bonding also observed between NH...N with bond distance of

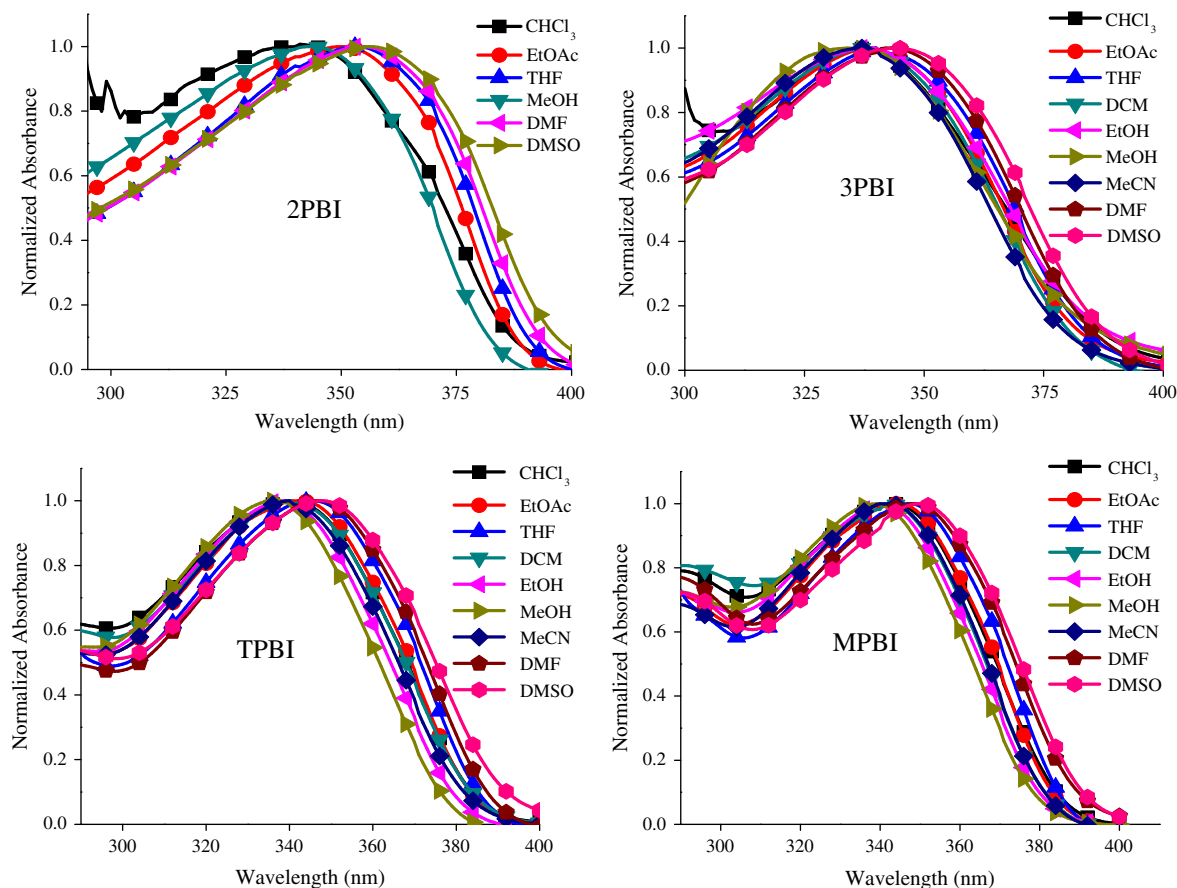


Fig. 4. UV-Vis normalized absorption spectra of imidazole derivatives 2PBI, 3PBI, TPBI and MPBI in series of solvents.

Table 2

Optical properties of imidazole derivatives in different solvents.

Solvents	$\lambda_{\text{abs}} (\text{nm})/\epsilon \times 10^3 \text{ M}^{-1} \text{ cm}^{-1}$				$\lambda_{\text{emi}} (\text{nm})$			
	2PBI	3PBI	TPBI	MPBI	2PBI	3PBI	TPBI	MPBI
CHCl ₃	340/–	336/38.1	340/44.2	343/29.5	441	442	432	433
EtOAc	350/–	340/–	342/37.8	345/40.6	433	436	433	432
THF	353/69.5	340/49.5	346/54.6	347/39.0	435	435	435	431
DCM	–/–	338/35.4	340/38.5	341/30.2	–	437	437	436
EtOH	–/–	338/–	339/38.1	340/63.7	–	453	446	449
MeOH	343/–	334/–	336/61.1	339/40.6	449	448	447	449
MeCN	–/–	337/–	340/82.2	340/33.9	–	463	449	449
DMF	354/62.4	343/44.7	347/43.7	348/46.5	454	463	449	452
DMSO	356/65.0	344/43.0	348/40.1	351/26.0	460	464	457	455

3.01 Å (Fig. 3). The bond angles of benzene ring and five member ring are juxtapose to 120° and 108° suggest that the π -electrons in the whole molecule are delocalized. The relevant crystal data of the compound is presented in Table 1.

3.3. UV–Vis absorption spectra

Preliminary efforts have been taken to gain insight into the photophysical properties of the fluorophores by investigating their absorption and emission behavior in various solvents with different polarity. Absorption spectra of all the compounds in various solvents are shown in Fig. 4, and the relevant spectral data are reported in Table 2. From Fig. 4, the absorption band below 300 nm is attributed to the π - π^* transition arising from the phenyl groups attached at C4 and C5 position of imidazole ring. The band around 334–356 nm with high intensity ($\epsilon = 26,000$ – $82,000 \text{ M}^{-1} \text{ cm}^{-1}$) in various solvents is attributed to the π - π^* transition arising from

conjugated-pyridine substituted phenyl groups attached to C2 position of imidazole ring. Importantly, the effect of solvent polarity on the absorption behavior is very minimal about 16 nm, 10 nm, 12 nm and 12 nm for 2PBI, 3PBI, TPBI and MPBI respectively. This suggests a less polar ground state which will be less effectively solvated by the polar solvents. On increasing the solvent polarity from CHCl₃ to DMSO, bathochromic shift was observed except for MeOH and EtOH. This abated bathochromic shift in polar protic solvents may be attributed to the hydrogen bonding interaction of solvent molecules with imidazole ring as well as pyridine moiety. This typical behavior can be ascribed to the increased solvent–solute interaction in polar protic solvents [33].

3.4. Fluorescence spectra

An emission behavior of the electronically excited fluorophores were also examined in a series of solvents with varying polarity to

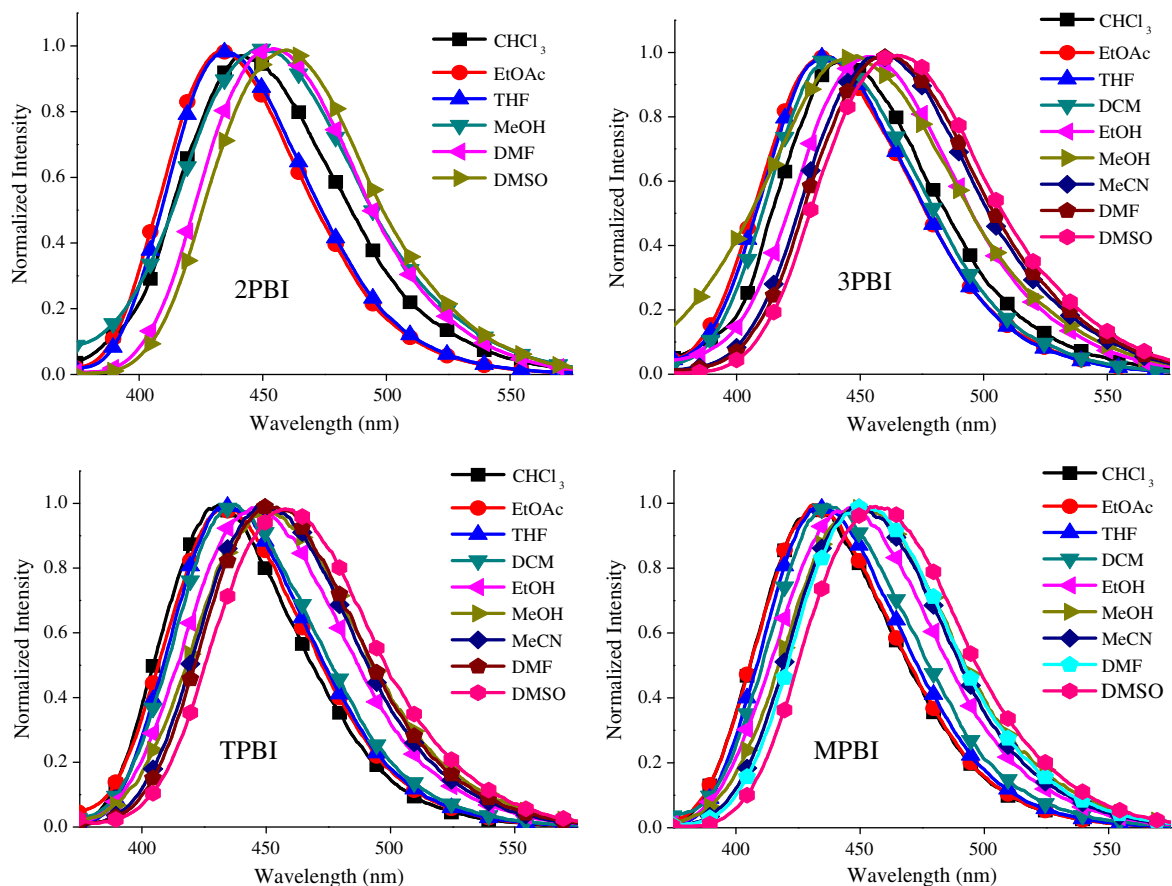


Fig. 5. Normalized emission spectra of imidazole derivatives 2PBI, 3PBI, TPBI and MPBI in series of solvents.

Table 3
Dipole moment, radius and electrochemical properties of the compounds.

Compounds	Dipole moment μ (D)			Radius (\AA)	$^{\circ}E^{\text{ox}}$ (V)	$^{\text{d}}E_{\text{g}}$ (eV)	$^{\text{e}}\text{HOMO}$ (eV)	$^{\text{e}}\text{LUMO}$ (eV)
	$\mu_{\text{g}}(\text{D})^{\text{a}}$	$\mu_{\text{e}}(\text{D})^{\text{b}}$	$\Delta\mu(\text{D})$					
2PBI	3.91	10.86	6.95	5.27	1.33	3.15	−5.53	−2.38
3PBI	6.13	16.77	10.64	5.27	1.33	3.21	−5.53	−2.32
TPBI	2.7	12.1	9.4	4.87	1.26	3.20	−5.46	−2.26
MPBI	2.8	12.6	9.8	4.73	1.23	3.18	−5.43	−2.25

^a Calculated by using AM1 analysis.

^b Calculated from the slope of Lippert Mataga equation.

^c Obtained from cyclic voltammetry measurements.

^d Estimated from onset of the absorption spectra $E_{\text{g}} = (1240)/\lambda_{\text{onset}}$.

^e The HOMO and LUMO energies were determined from cyclic voltammetry and the absorption onset. Ferrocene (4.8 eV) was used as the internal standard in each experiment. The ferrocene oxidation potential was located at +600 mV, relative to the saturated Ag/AgCl reference electrode.

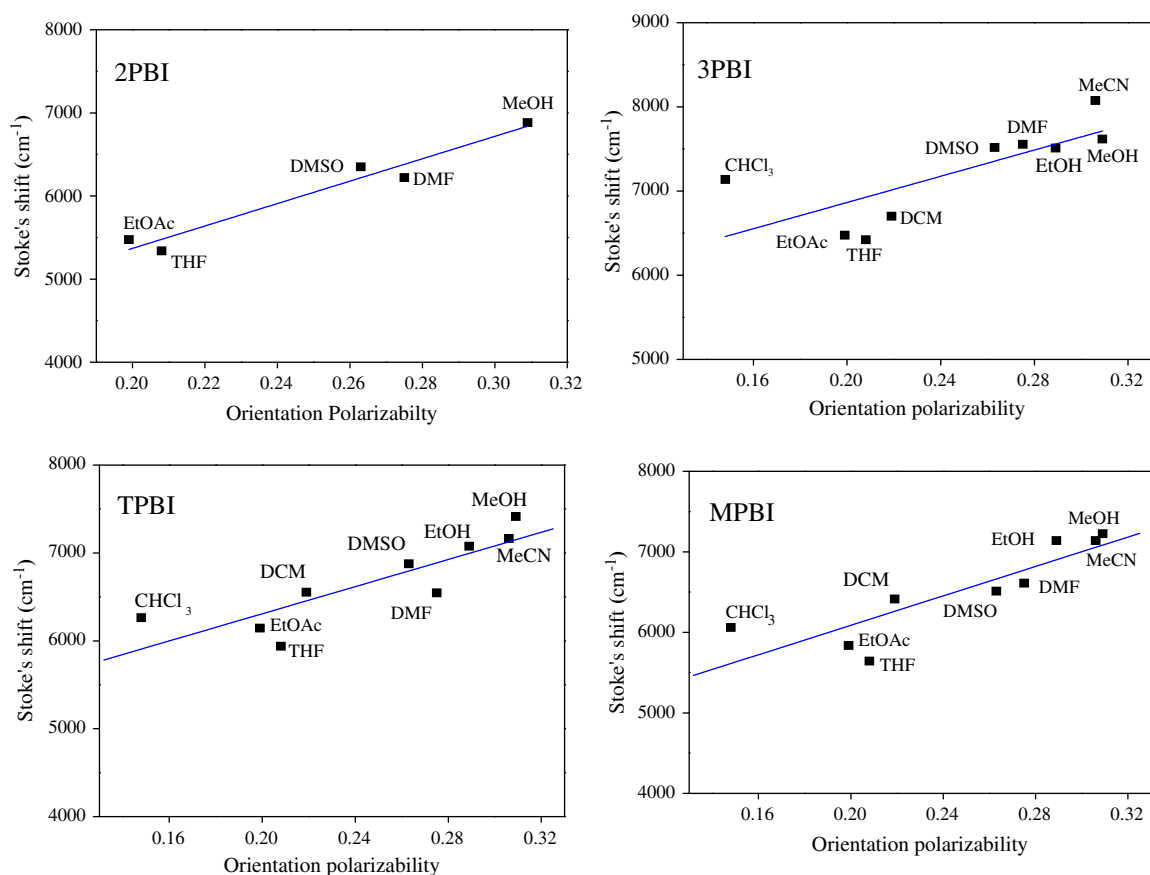


Fig. 6. Lippert–Mataga plots of imidazole derivatives 2PBI, 3PBI, TPBI and MPBI in series of solvents.

identify the impact of solvent polarity on the excited state and also to identify the nature of molecules in the excited state. Representative illustrations showing the influence of the solvent polarity on the emission profile are displayed in Fig. 5 for the fluorophores. The emission profile of the fluorophores exhibited a positive solvatochromism with more bathochromically shifted emission maxima in the polar solvents such as MeCN, DMF and DMSO which led to the gradual increase in the Stoke shift on increasing the solvent polarity.

The extent of charge separation on electronic excitation of compounds were quantified by measuring the change in the dipole moment ($\Delta\mu = \mu_{\text{e}} - \mu_{\text{g}}$) utilizing the shift between the absorption and emission maxima $\Delta\nu = (\nu_{\text{abs}} - \nu_{\text{em}})$ as a function of solvent polarity. According to the Lippert–Mataga [20,34,35] Eq. (4).

Table 4

Quantum yield (ϕ_f), Stokes shift ($\Delta\nu$), orientation polarizability (Δf) values in different solvents.

Solvents	ϕ_f				$\Delta\nu$ (cm^{-1})				Δf
	2PBI	3PBI	TPBI	MPBI	2PBI	3PBI	TPBI	MPBI	
CHCl ₃	0.88	0.27	0.69	0.66	6736	7137	6554	6416	0.219
EtOAc	0.74	0.66	0.81	0.88	5476	6475	6546	6611	0.275
THF	0.44	0.63	0.79	0.84	5340	6423	7164	7140	0.306
DCM	–	0.49	0.88	0.60	–	6702	7415	7226	0.309
EtOH	–	0.46	0.32	0.46	–	7510	7077	7140	0.289
MeOH	0.38	0.31	0.28	0.32	6882	7618	6263	6059	0.148
MeCN	–	0.65	0.41	0.87	–	8075	6145	5837	0.199
DMF	0.70	0.65	0.87	0.88	6222	7556	5939	5643	0.208
DMSO	0.64	0.64	0.79	0.77	6350	7518	6877	6512	0.263

Table 5

Estimated from equation x coefficients (y_0 , a_{SA} , b_{SB} , c_{SP} , d_{SDP}), their correlation coefficients (r) for the multiple linear regression analysis of E(A), E(F) and E(S) of the compounds as a function of the Catalán four-parameter solvent scale.

y	y_0 (kcal/mol)	a_{SA}	b_{SB}	c_{SP}	d_{SDP}	r
2PBI						
E_{abs}	88.55	2.31	-6.40	-5.42	0.21	0.9996
E_{emi}	74.23	-1.15	0.78	-6.53	-6.98	0.9960
E_{st}	14.32	3.47	-7.19	1.10	7.19	0.9952
3PBI						
E_{abs}	88.77	2.15	-2.63	-4.06	-0.74	0.9714
E_{emi}	71.51	0.86	-0.55	-0.01	-9.48	0.8118
E_{st}	17.26	1.28	-2.07	-4.05	8.73	0.7952
TPBI						
E_{abs}	89.13	2.78	-2.97	-5.77	-0.54	0.9741
E_{emi}	71.94	-0.67	-1.36	-1.87	-6.56	0.9534
E_{st}	17.18	3.45	-1.61	-3.89	6.02	0.9394
MPBI						
E_{abs}	89.22	1.87	-2.98	-7.42	0.45	0.9350
E_{emi}	72.15	-1.50	-1.01	-1.58	-7.15	0.9357
E_{st}	17.07	3.37	-1.97	-5.83	7.60	0.9189

Table 6

Correlation of E(A), E(F) and E(S) with Taft's π^* (solvent dipolarity/polarisability), α and β (hydrogen bond donating and accepting ability of the solvent) values based on multiple linear regression analysis (Kamlet-Taft).

y	y_0 (kcal/mol)	$\alpha\alpha$	$b\beta$	$c\pi^*$	r
2PBI					
E_{abs}	83.11	2.84	-3.03	-0.43	0.996
E_{emi}	70.83	-2.24	-0.18	-8.63	0.998
E_{st}	12.28	5.08	-2.84	8.21	0.995
3PBI					
E_{abs}	85.33	1.51	-1.13	-1.3	0.926
E_{emi}	70.31	-1.53	-2.31	-7.27	0.787
E_{st}	15.07	3.05	1.17	5.97	0.692
TPBI					
E_{abs}	84.23	2.23	-1.14	-1.04	0.925
E_{emi}	70.26	-1.55	-2.31	-5.94	0.936
E_{st}	13.97	3.78	1.17	4.89	0.861
MPBI					
E_{abs}	83.5	2.15	-1.09	-0.573	0.874
E_{emi}	70.86	-2.28	-2.46	-6.42	0.925
E_{st}	12.64	4.43	1.37	5.84	0.852

$$v_{abs} - v_{em} = \Delta v = \frac{2}{hca^3} (\mu_e - \mu_g)^2 \Delta f + \text{Constant} \quad (4)$$

where

$$\Delta f = \frac{s-1}{2s+1} - \frac{n^2-1}{2n^2+1} \quad (5)$$

where Δv is the Stokes shift, μ_g and μ_e are ground and excited state dipole moments, c is the velocity of light, h is the Planck's constant, and a is the Onsager cavity radius swept out by the fluorophore. A plot of Δv versus Δf gives $\Delta\mu$ from the slope. Using the mole inspiration software, the volume of the compounds is measured. By using the volume, Onsager cavity radius has been calculated which are reported in Table 3. From the DFT calculations at the B3LYP/6-311G(d,p) level, the ground state dipole moment (μ_g) is obtained. The values of μ_g for the compounds 2PBI, 3PBI, TPBI and MPBI are 3.9 D, 6.1 D, 2.7 D and 2.8 D respectively. The positive slope of the Lippert Metaga plot (Δv versus Δf) in the solvents studied suggest that general solvent effects are responsible for the observed positive solvatochromic shifts in emission (Fig. 6). The dipole moment change on excitation is estimated from the slope of Eq(4) to be around 10.8 D, 16.7 D, 12.1 D and 12.6 D for 2PBI, 3PBI, TPBI and MPBI respectively (Table 3). Notably, the change in position of N atom drastically changes the dipole moment in both ground and excited state. Substantially, high values of μ_e thus obtained from plot suggest that the fluorescence states of all these compounds are of highly polar in nature. The fluorophores, in general, showed moderate quantum efficiencies in less polar and high polar aprotic solvents (Table 4). However, the quantum efficiencies are decreased in polar protic solvents such as MeOH and EtOH which may be ascribed to the increased solvent-solute hydrogen bonding interactions that presumably responsible for lowering of Φ_f efficiencies.

3.5. Multi-linear regression analysis

Multi-parameter correlation is an excellent and preferable method to analyze the various factors (acidity, basicity, polarisability and dipolarity) that affecting the photophysical properties of the compounds and which has been applied successfully to various physicochemical parameters. The most frequently used solvent scales are those of Kamlet and Taft, and Catalán. The new four-parameter Catalán solvent scale has an advantage over other solvent scales. Hence, herein the spectral and photophysical parameters of the compounds studied in all solvents used will be

discussed based on the four-parameter Catalán solvent scale. However, the correlations obtained using Kamlet-Taft solvent scale are also presented (Table 6) and will be compared with each other.

The estimated coefficients and correlation coefficients (r) for the multi-linear regression analysis of absorption (E_{abs}) and fluorescence (E_{emi}) maxima and Stokes shift (ΔE) of the compounds using the four parameter Catalán and Kamlet-Taft solvent polarity scale are collected in Tables 5 and 6. A fair fit was obtained for the dependence of maxima of absorption (E_{abs}) ($r = 0.9996-0.9350$) in which all four coefficients are significant (Table 5). However, the large value of the c_{SP} coefficient compared to others (a_{SA} , b_{SB} and d_{SDP}) indicates that the change of (E_{abs}) may reflect primarily a change in polarizability of the environment of the fluorophore. Solvent acidity and basicity also affect the position of the absorption maxima but to a smaller degree than its polarizability except for 2PBI. Whereas, the influence of solvent acidity and basicity on E_{abs} is higher than the dipolarity/polarizability (π^*) in the three-parameter solvent polarity scale (Kamlet-Taft).

The fit of (E_{emi}) as a function of SP, SdP, SA, SB is satisfactory, as judged by the value of r as the quality-of-fit criterion, for the compounds 2PBI, TPBI and MPBI ($r = 0.9996-0.9357$) but which is low for 3PBI ($r = 0.8118$). Solvent polarizability and dipolarity both have effect on E_{emi} of the 2PBI. However, solvent dipolarity (SdP) alone have major impact on change in E_{emi} for 3PBI, TPBI and MPBI. Also, it is worth mentioning that the coefficient values are negative meaning that their changes cause red-shift of the fluorescence maximum. This indicates that the electronic structure of the Franck-Condon and relaxed excited state of the compounds differ significantly, and the relaxed excited state is more polar, which is consistent with a higher excited state dipole moment than the ground state [36]. For instance, the SdP coefficients of 3PBI are much more which is reflected in high excited state dipole moment compared with others. Application of the three-parameter solvent scale also gives similar dependences (high π^* values). Correlation of the Stokes shift of 2PBI with the four-parameter solvent scale indicates that both solvent basicity (SB) and dipolarity (SdP) plays equally on changing the absorption and emission maxima with good fitting parameter ($r = 0.9952$). But spectral behavior of other compounds such as 3PBI, TPBI and MPBI mainly influenced by solvent dipolarity with some contribution of solvent polarizability. For all the compounds, the correlations with three parameter solvent scales indicate low influence of basicity of the solvent and mutual influence of acidity and dipolarity/polarisability.

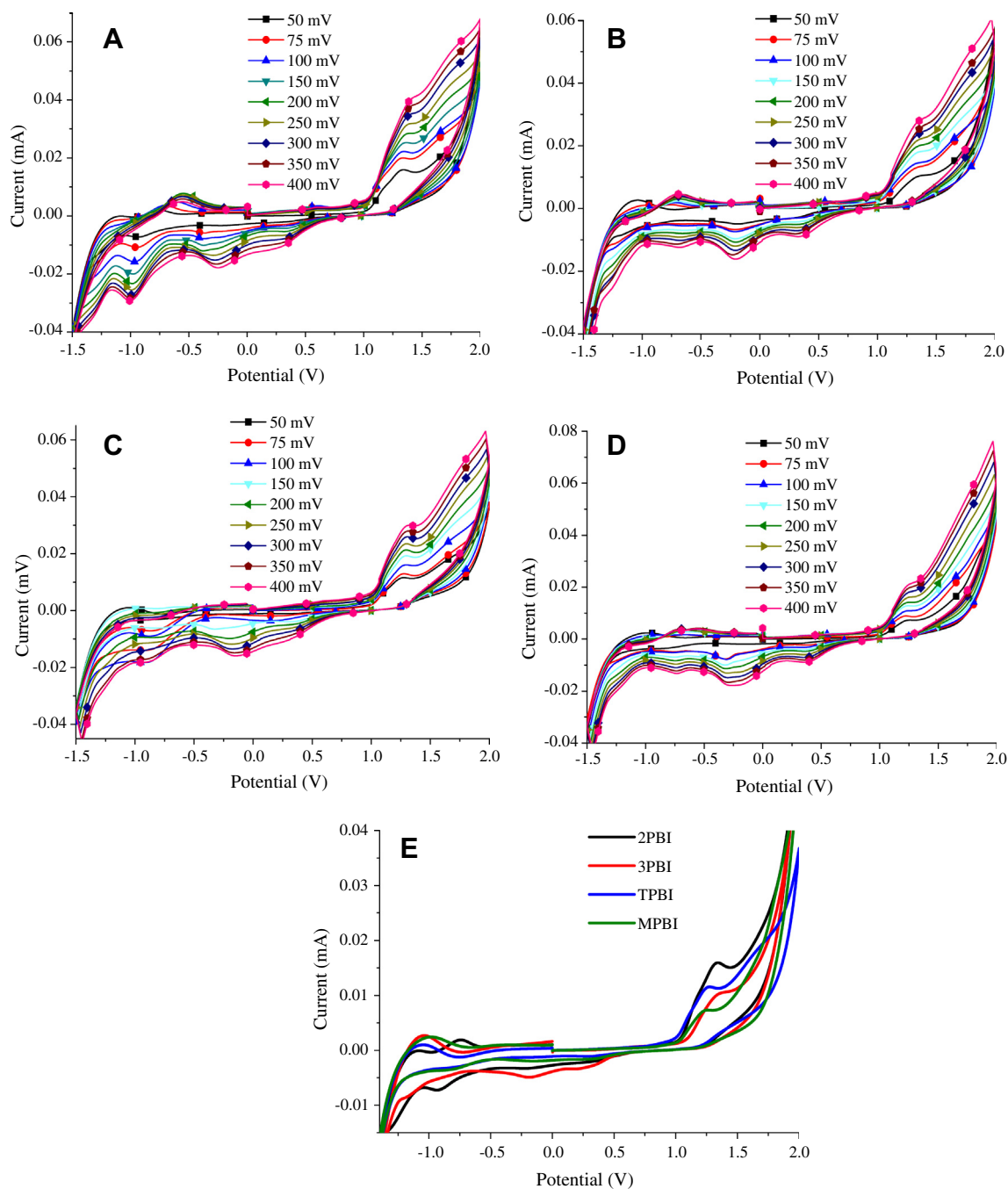


Fig. 7. Cyclic voltammogram of 2PBI (A), 3PBI (B), TPBI (C) and MPBI (D) with varying scan rate in DMF, all the compounds (E) at 100 mV scan rate in DMF.

3.6. Electrochemical properties

The electrochemical properties of the new fluorophores were examined by using cyclic voltammetry (CV) measurements in a three-electrode cell setup with 0.1 M TBAPF₆ as the supporting electrolyte and ferrocene (Fc) as the internal standard. Representative cyclic voltammograms are shown in Fig. 7. The details of the electrochemical properties of these compounds are listed in Table 3. A quasi irreversible oxidation and reduction wave observed for all the compounds and is attributed to the oxidation and regeneration of the imidazole based conjugated spacer. This is consistent with results reported in the literature for the electrochemical behavior of imidazole and its derivatives [37]. The HOMO energy levels of these

materials were calculated with reference to ferrocene (4.8 eV), which are ranging from -5.43 to -5.53 eV. The LUMO energy levels were calculated from HOMO energy and band gap derived from the absorption edge and ranges from -2.25 to -2.38 eV (Table 3). The electrochemical stability of the compounds were examined using cyclic voltammetric analysis (Fig. 7) in DMF by measuring repeated cycles with varying scan rate. All the compounds showed completely stable peaks for the entire scanning rate in the region from 50 mV s^{-1} to 400 mV s^{-1} . A plot of the peak current against the square root of scan rate was found to be linear as shown in Fig. 8 for all the compound ($R^2 = 0.9943$ – 0.9949 , in DMF), which describes an excellent electrolyte ion diffusion behavior of electrochemical property of the compounds even at high scan rates [38].

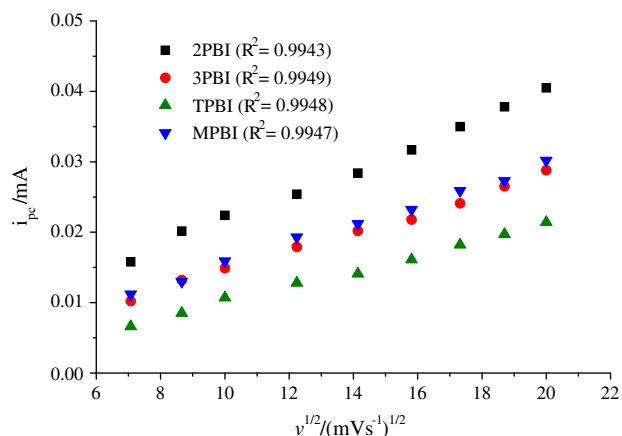


Fig. 8. Plots of the cathodic peak current versus the square root of the scan rate for the compounds in DMF.

3.7. Fluorescence imaging studies

Further we were interested to utilize the fluorescence property of the compounds to probe the microbes by using fluorescence microscopy. For that, we selected one of the compounds which is having high quantum efficiency in most of the solvents namely MPBI. *E. coli* culture was incubated with the compound MPBI (1:1 v/v) for 5 h at 37 °C and washed with phosphate buffered saline (PBS – pH 7.4), three times to remove any unbound fluorophore. Individual aliquots of 50 μ l were withdrawn and placed over microscopic slides and observed under a microscope after air drying. Fig. 9 displays the results of fluorescence microscopy. From Fig. 9, an untreated *E. coli* could not be detectable (Fig. 9a), but MPBI treated plates showed deep blue color image of *E. coli*. The possible mode of binding nature of the fluorophore with the bacteria could be the hydrogen bond interaction between the imidazole moieties with amino acid groups of peptidoglycan cell wall of bacteria.

3.8. Antimicrobial and antifungal studies

The data generated from this study (Table 7) revealed that the synthesized compounds (3PBI, TPBI and MPBI) showed variable

Table 7

In vitro antibacterial and antifungal activity of compounds analyzed by disc diffusion method.

Compound	Gram-negative bacteria			Gram-positive bacteria	Fungus
	<i>E. coli</i>	<i>P. aeruginosa</i>	<i>A. hydrophila</i>	<i>R. rhodochrous</i>	<i>C. albicans</i>
	MTCC 2939	MTCC 1934	MTCC 1739	MTCC 265	MTCC 227
3PBI ^a	12	08	14	13	16
TPBI ^a	11	13	13	14	07
MPBI ^a	14	14	12	10	08
Erythromycin ^b	32	25	30	24	–
Itraconazole ^c	–	–	–	–	07

^a 30 μ l/disc.

^b 15 mcg/disc.

^c 10 mcg/disc, Zone of inhibition in mm, All results were expressed triplicate.

inhibition activities against the tested strains and all of them showed moderate to good antibacterial and antifungal activity as compared to that of the standard. Of all the compounds tested in series, MPBI showed significant inhibition against Gram-negative strains and TPBI against Gram-positive strains. The antifungal screening data (Table 7) revealed that all the tested compounds showed significant fungal inhibition. Compound 3PBI exhibited very high antifungal activity against fungal strain (*C. albicans*, MTCC 227). This can be ascribed to the presence of two biologically important imidazole moieties, hence the activity was found to be twice than that of the standard itraconazole. Similarly, other compounds (TPBI and MPBI) also exhibited moderate activity against fungal strain as compared to that of the standard. These results suggest that the synthesized compounds found to be the most effective antifungal agents.

4. Conclusions

Highly fluorescent imidazole-pyridine derivatives were synthesized by using Suzuki coupling and multicomponent cyclization reactions. Effect of solvent polarity on absorption behavior was minimal which suggested a less polar ground state. Bathochromic shift of fluorescence spectra of the compounds on increasing solvent polarity demonstrated that excited state were more sensitive

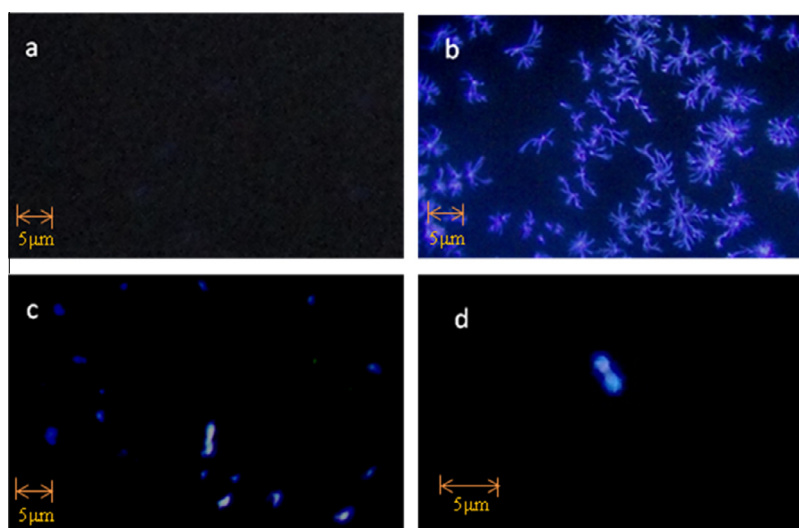


Fig. 9. Fluorescent micrographs of MPBI treated and untreated *E. coli*. (a) Fluorescent micrograph of *E. coli*. (b) Fluorescent micrograph of compound (MPBI). (c) Fluorescent micrograph of MPBI treated *E. coli*. (d) Fluorescent micrograph of MPBI treated *E. coli* (zoomed view).

to the polarity of the microenvironment. Increased dipole moment obtained by Lippert–Metaga plot suggests more polar nature of excited state. In addition, multi linear regression analysis based on Kamlet–Taft and Catalán new four parameter solvent scale results in observed solvatochromism was mainly influenced by solvent polarisability and dipolarity of the environment. Excellent electrolyte ion diffusion behavior with stable electrochemical property of the compounds was explored. High quantum efficiencies of the compounds were successfully utilized to probe the bacteria by using fluorescence microscopy. The biological activity analysis of the compounds revealed that these fluorophore exhibit notable inhibitions against the bacteria (MPBI and TPBI) and *C. albicans* (3PBI).

Acknowledgements

N. N thanks DST-INSPIRE program for the financial assistant as a JRF (IF10495). R. R thanks DST, India, for their financial support in the form of a research grant (Ref. No. SR/S1/PC-12/2011, dt. 20/09/2011). T. S thanks University Grants Commission (UGC), New Delhi, India for their financial support.

References

- [1] R.J. Sundberg, R.B. Martin, Interactions of histidine and other imidazole derivatives with transition metal ions in chemical and biological systems, *Chem. Rev.* 74 (1974) 471–517.
- [2] I.M. Pastor, M. Yus, Bioactive N-phenylimidazole derivatives, *Curr. Chem. Biol.* 3 (2009) 65–88.
- [3] C. Hardacre, J.D. Holbrey, S.E.J. McMath, A highly efficient synthetic procedure for deuterating imidazoles and imidazolium salts, *Chem. Commun.* (2001) 367–368.
- [4] M. Velusamy, Y.-C. Hsu, J.T. Lin, C.-W. Chang, C.-P. Hsu, 1-Alkyl-1H-imidazole-based bipolar organic compounds for dye-sensitized solar cells, *Chem. Asian J.* 5 (2010) 87–96.
- [5] D. Kumar, K.R.J. Thomas, C.-P. Lee, K.-C. Ho, Novel pyrenoimidazole-based organic dyes for dye-sensitized solar cells, *Org. Lett.* 13 (2011) 2622–2625.
- [6] E.M. Cross, K.M. White, R.S. Moshrefzadeh, C.V. Francis, Azobenzimidazole compounds and polymers for nonlinear optics, *Macromolecules* 28 (1995) 2526–2532.
- [7] J. Santos, E.A. Mintz, O. Zehnder, C. Bosshard, X.R. Bu, P. Günter, New class of imidazoles incorporated with thiophenevinyl conjugation pathway for robust nonlinear optical chromophores, *Tetrahedron Lett.* 42 (2001) 805–808.
- [8] K. Feng, L. De Boni, L. Misoguti, C.R. Mendonca, M. Meador, F.-L. Hsu, X.R. Bu, Y-shaped two-photon absorbing molecules with an imidazole-thiazole core, *Chem. Commun.* (2004) 1178–1180.
- [9] J. Kulhánek, F. Bureš, T. Mikysek, J. Ludvík, O. Pytela, Imidazole as a central π -linkage in Y-shaped push–pull chromophores, *Dyes Pigm.* 90 (2011) 48–55.
- [10] Z. Wang, P. Lu, S. Chen, Z. Gao, F. Shen, W. Zhang, Y. Xu, H.S. Kwok, Y. Ma, Phenanthro[9,10-d]imidazole as a new building block for blue light emitting materials, *J. Mater. Chem.* 21 (2011) 5451–5456.
- [11] X. Yang, S. Zheng, R. Bottger, H.S. Chae, T. Tanaka, S. Li, A. Mochizuki, G.E. Jabbar, Efficient fluorescent deep-blue and hybrid white emitting devices based on carbazole/benzimidazole compound, *J. Phys. Chem. C* 115 (2011) 14347–14352.
- [12] H. Huang, X. Yang, B. Pan, L. Wang, J. Chen, D. Ma, C. Yang, Benzimidazole-carbazole-based bipolar hosts for high efficiency blue and white electrophosphorescence applications, *J. Mater. Chem.* 22 (2012) 13223–13230.
- [13] Z.M. Wang, X.H. Song, Z. Gao, D.W. Yu, X.J. Zhang, P. Lu, F.Z. Shen, Y.G. Ma, Tuning of the electronic and optical properties of 4,4'-bis(1-phenylphenanthro[9,10-d]imidazol-2-yl)biphenyl via cyano substitution in un-conjugated phenyl, *RSC Adv.* 2 (2012) 9635–9642.
- [14] M. Alfonso, A. Tárraga, P. Molina, A bisferrocene-benzobisimidazole triad as a multichannel ditopic receptor for selective sensing of hydrogen sulfate and mercury ions, *Org. Lett.* 13 (2011) 6432–6435.
- [15] M.a. Alfonso, A. Espinosa, A. Tárraga, P. Molina, A simple but effective dual redox and fluorescent ion pair receptor based on a ferrocene–imidazopyrene dyad, *Org. Lett.* 13 (2011) 2078–2081.
- [16] D.Y. Lee, N. Singh, M.J. Kim, D.O. Jang, Chromogenic and fluorescent recognition of iodide with a benzimidazole-based tripodal receptor, *Org. Lett.* 13 (2011) 3024–3027.
- [17] P. Molina, A. Tárraga, F. Oton, Imidazole derivatives: a comprehensive survey of their recognition properties, *Org. Biomol. Chem.* 10 (2012) 1711–1724.
- [18] S. Sangeetha, G. Sathiyaraj, D. Muthamilselvan, V.G. Vaidyanathan, B.U. Nair, Structurally modified 1,10-phenanthroline based fluorophores for specific sensing of Ni²⁺ and Cu²⁺ ions, *Dalton Trans.* 41 (2012) 5769–5773.
- [19] S. Park, J.E. Kwon, S.Y. Park, Strategic emission color tuning of highly fluorescent imidazole-based excited-state intramolecular proton transfer molecules, *Phys. Chem. Chem. Phys.* 14 (2012) 8878–8884.
- [20] D. Kumar, K.R.J. Thomas, Optical properties of pyrene and anthracene containing imidazoles: experimental and theoretical investigations, *J. Photochem. Photobiol. A* 218 (2011) 162–173.
- [21] T.P.T. Cushnie, A.J. Lamb, Antimicrobial activity of flavonoids, *Int. J. Antimicrob. Agents* 26 (2005) 343–356.
- [22] Z.A. Kaplancıklı, G. Turan-Zitouni, A. Özdemir, G. Reviel, New triazole and triazolothiadiazine derivatives as possible antimicrobial agents, *Eur. J. Med. Chem.* 43 (2008) 155–159.
- [23] J.V. Morris, M.A. Mahaney, J.R. Huber, Fluorescence quantum yield determinations. 9,10-Diphenylanthracene as a reference standard in different solvents, *J. Phys. Chem.* 80 (1976) 969–974.
- [24] M.J. Kamlet, J.L. Abboud, R.W. Taft, The solvatochromic comparison method. 6. The π^* scale of solvent polarities, *J. Am. Chem. Soc.* 99 (1977) 6027–6038.
- [25] M.J. Kamlet, J.L.M. Abboud, M.H. Abraham, R.W. Taft, Linear solvation energy relationships. 23. A comprehensive collection of the solvatochromic parameters, π^* , α , and β , and some methods for simplifying the generalized solvatochromic equation, *J. Org. Chem.* 48 (1983) 2877–2887.
- [26] J. Catalán, Toward a generalized treatment of the solvent effect based on four empirical scales: dipolarity (SdP, a New Scale), polarizability (SP), acidity (SA), and basicity (SB) of the medium, *J. Phys. Chem. B* 113 (2009) 5951–5960.
- [27] A. Filarowski, M. Kluba, K. Cieslik-Boczuła, A. Koll, A. Kochel, L. Pandey, W.M. De Borggraeve, M. Van der Auweraer, J. Catalan, N. Boens, Generalized solvent scales as a tool for investigating solvent dependence of spectroscopic and kinetic parameters. Application to fluorescent BODIPY dyes, *Photochem. Photobiol. Sci.* 9 (2010) 996–1008.
- [28] N. Kuhnert, C. Patel, F. Jami, Synthesis of chiral nonracemic polyimine macrocycles from cyclocondensation reactions of biaryl and terphenyl aromatic dicarboxaldehydes and 1R,2R-diaminocyclohexane, *Tetrahedron Lett.* 46 (2005) 7575–7579.
- [29] A. Puglisi, M. Benaglia, G. Roncan, Palladium-catalyzed synthesis of nonsymmetrically functionalized bipyridines, poly(bipyridines) and terpyridines, *Eur. J. Org. Chem.* 2003 (2003) 1552–1558.
- [30] A. Rameshkumar, T. Sivasudha, R. Jeyadevi, B. Sangeetha, D.A. Ananth, G.S.B. Aseervatham, N. Nagarajan, R. Renganathan, A. Kathiravan, In vitro antioxidant and antimicrobial activities of *Merremia emarginata* using thio glycolic acid-capped cadmium telluride quantum dots, *Colloid Surf. B* 101 (2013) 74–82.
- [31] F.R. Japp, H.H. Robinson, Constitution des Lophins und des Amarins, *Berichte der deutschen chemischen Gesellschaft* 15 (1882) 1268–1270.
- [32] B. Radziszewski, Ueber die Constitution des Lophins und verwandter Verbindungen, *Berichte der deutschen chemischen Gesellschaft* 15 (1882) 1493–1496.
- [33] S. Dhar, S. Singha Roy, D.K. Rana, S. Bhattacharya, S. Bhattacharya, S.C. Bhattacharya, Tunable solvatochromic response of newly synthesized antioxidative naphthalimide derivatives: intramolecular charge transfer associated with hydrogen bonding effect, *J. Phys. Chem. A* 115 (2011) 2216–2224.
- [34] S. Pramanik, P. Banerjee, A. Sarkar, A. Mukherjee, K.K. Mahalanabis, S.C. Bhattacharya, Spectroscopic investigation of 3-pyrazolyl 2-pyrazoline derivative in homogeneous solvents, *Spectrochim. Acta, Part A* 71 (2008) 1327–1332.
- [35] G.V. Loukova, A.A. Milov, V.P. Vasiliev, V.A. Smirnov, Dipole moment of a metallocene precatalyst in the ground and excited states, *Russ. Chem. Bull.* 57 (2008) 1166–1171.
- [36] K. Guzow, M. Czerwinska, A. Cezlak, M. Kozarzewska, M. Szabelski, C. Czaplowski, A. Lukaszewicz, A.A. Kubicki, W. Wiczak, Photophysical properties of 3-[2-(N-phenylcarbazolyl)benzoxazol-5-yl]alanine derivatives – experimental and theoretical studies, *Photochem. Photobiol. Sci.* 12 (2013) 284–297.
- [37] N.-t. Zhang, C.-c. Zeng, C.M. Lam, R.K. Gbur, R.D. Little, Triarylimidazole redox catalysts: electrochemical analysis and empirical correlations, *J. Org. Chem.* 78 (2013) 2104–2110.
- [38] A. Shah, E. Nosheen, S. Munir, A. Badshah, R. Qureshi, Z.-u. Rehman, N. Muhammad, H. Hussain, Characterization and DNA binding studies of an unexplored imidazolidines by electronic absorption spectroscopy and cyclic voltammetry, *J. Photochem. Photobiol. B* 120 (2013) 90–97.